XML-IS

Our reference: BM 5368 P-authorquery-vx

AUTHOR QUERY FORM

ELSEVIER	**Journal: BM** **Article Number: 5368**	**Please e-mail or fax your responses and any corrections to:** **E-mail: corrections.eseo@elsevier.macipd.com** **Fax: +44 1392 285878**

Dear Author,

Please check your proof carefully and mark all corrections at the appropriate place in the proof (e.g., by using on-screen annotation in the PDF file) or compile them in a separate list.

For correction or revision of any artwork, please consult http://www.elsevier.com/artworkinstructions.

Any queries or remarks that have arisen during the processing of your manuscript are listed below and highlighted by flags in the proof. Click on the Q link to go to the location in the proof.

Location in article	Query / Remark: click on the Q link to go Please insert your reply or correction at the corresponding line in the proof
Q1	Please confirm that given names and surnames have been identified correctly.
Q2	Reference(s) given here were noted in the reference list but are missing from the text – please position each reference in the text or delete it from the list.
Q3	The citation "Rivlin (1948)" has been changed to match the author name/date in the reference list. Please check here and in subsequent occurrences, and correct if necessary.
Q4	Please note that the reference style has been changed from a Numbered style to a Name-Date style as per the journal specifications.
Q5	Please check the author group in the Ref. "Holzapfel and Ogden, 2009".
Q6	Please check the significance of * in the tables 2,3, and 4 and correct if necessary.

Thank you for your assistance.

Journal of Biomechanics ▮ (▮▮▮▮) ▮▮▮–▮▮▮

Contents lists available at SciVerse ScienceDirect

Journal of Biomechanics

journal homepage: www.elsevier.com/locate/jbiomech
www.JBiomech.com

Biomechanical wall properties of Human intracranial aneurysms resected following surgical clipping (IRRAs Project)☆

V. Costalat*, M. Sanchez, D. Ambard, L. Thines, N. Lonjon, F. Nicoud, H. Brunel, J.P. Lejeune, H. Dufour, P. Bouillot, J.P. Lhaldky, K. Kouri, F. Segnarbieux, C.A. Maurage, K. Lobotesis, M.C. Villa-Uriol, C. Zhang, A.F. Frangi, G. Mercier, A. Bonafé, L. Sarry, F. Jourdan

CHU Montpellier, Interventional Neuroradiology, Av Augstin Fliche, Montpellier, France

ARTICLE INFO

Article history:
Accepted 28 July 2011

Keywords:
Intracranial aneurysm
Soft tissue
Hyperelastic material
Rupture risk
human specimen
Uniaxial traction test

ABSTRACT

Background and purpose: Individual rupture risk assessment of intracranial aneurysms is a major issue in the clinical management of asymptomatic aneurysms. Aneurysm rupture occurs when wall tension exceeds the strength limit of the wall tissue. At present, aneurysmal wall mechanics are poorly understood and thus, risk assessment involving mechanical properties is inexistent. Additionally, aneurysmal computational hemodynamics usually makes the assumption of rigid walls, an arguable simplification. We therefore aim to assess mechanical properties of ruptured and unruptured intracranial aneurysms in order to provide the foundation for future patient-specific aneurysmal risk assessment. This work will also challenge some of the currently held hypotheses in computational flow hemodynamics research.

Methods: A specific conservation protocol was applied to aneurysmal tissues following clipping and resection in order to preserve their mechanical properties**. Sixteen intracranial** aneurysms (11 female, 5 male) underwent mechanical uniaxial stress tests under physiological conditions, temperature, and saline isotonic solution. These represented 11 unruptured and 5 ruptured aneurysms. Stress/strain curves were then obtained for each sample, and a fitting algorithm was applied following a 3-parameter (C_{10}, C_{01}, C_{11}) Mooney–Rivlin hyperelastic model. Each aneurysm was classified according to its biomechanical properties and (un)rupture status.

Results: Tissue testing demonstrated three main tissue classes: Soft, Rigid, and Intermediate. All unruptured aneurysms presented a more Rigid tissue than ruptured or pre-ruptured aneurysms within each gender subgroup. Wall thickness was not correlated to aneurysmal status (ruptured/unruptured). An Intermediate subgroup of unruptured aneurysms with softer tissue characteristic was identified and correlated with multiple documented risk factors of rupture.

Conclusion: A significant biomechanical properties modification between ruptured aneurysm, presenting a soft tissue and unruptured aneurysms, presenting a rigid material was observed. This finding strongly supports the idea that a biomechanical-based risk factor can and should be developed in the near future to improve the therapeutic decision making.

1. Introduction

The prevalence of unruptured intracranial aneurysms in the general population, as reported by a recent review, (Wardlaw and White, 2000) ranges between 3% and 6.6%. The incidence of ruptured aneurysms is however, low, with approximately 0.5% per year suggesting that very few aneurysms rupture. Subarachnoid hemorrhage is the consequence of aneurysm rupture and approximately 12% of patients die before receiving medical attention, 40% of hospitalized patients die within one month after the event, and more than one third of those who survive have major neurological deficits. In contrast endovascular treatment of unruptured aneurysms is safe with less than 1% mortality rate (Sluzewski et al., 2001). Unruptured intracranial aneurysms represent a dilemma for the physicians. The risks of aneurysm rupture with respect to its natural history against the risk of morbidity and mortality from an endovascular or surgical repair has to be carefully balanced. With brain imaging being more frequently and widely used, a growing number of intracranial aneurysms are being diagnosed, posing the problem of which aneurysms harbor a sufficiently high risk of rupture to

☆The research consortium "**I**ndividual **R**isk **R**upture **As**sessment of Intracranial aneurysm" (IRRAs) was found by 4 clinical centers, and 3 European laboratories in France, and Spain.

* Corresponding author.
E-mail address: vincentcost@hotmail.com (V. Costalat).

0021-9290/$ - see front matter © 2011 Published by Elsevier Ltd.
doi:10.1016/j.jbiomech.2011.07.026

merit endovascular or surgical repair. Recent publications have addressed this issue and have demonstrated that, among other variables affecting the natural history of aneurysms, aneurysm size and location represent independent predictors of rupture risk (Anonymos, 1998). Other parameters, such as irregular aneurysm shape and, in particular, the presence of blebs (Asari and Ohmoto, 1993; Wiebers et al., 1987) are recognized as high risk factors.

Rupture of an aneurysm occurs when wall tension exceeds the strength limit of the wall tissue. The ideal approach to risk assessment would therefore be to determine tension and material strength limits of the tissue (Kyriacou and Humphrey, 1996) in the aneurysmal wall. Individual aneurysmal material strength is impossible to measure non-invasively, but wall tension can be estimated using computational simulation (Isaksen et al., 2008). Over the last decade, a number of authors have shown that computational fluid dynamic simulations based on patient-specific anatomical models derived from medical imagery may be used to assess wall shear stress (WSS) and pressure in the Circle of Willis (Alnaes et al., 2007; Cebral et al., 2005; Radaelli et al., 2008). Others have used the same approach to analyze cerebral aneurysms, with particular focus on WSS, which is thought to be associated with aneurysm formation and risk rupture (Hoi et al., 2004; Cebral et al., 2011; Cebral et al., 2011). Although simulation of aneurysmal wall tension is now feasible in principle, real human aneurysmal wall biomechanical properties are still rarely explored in the literature (Scott et al., 1972; Toth et al., 2007). Computational simulations must be based on reliable material properties and boundaries. As opposed to hemodynamic boundary conditions that may be assessed by Phase Contraste-MRI or transcranial Doppler, in vivo, patient-specific measurements of tissue properties are not feasible yet. .Most of the current research on computational hemodynamics assumes uniform wall thickness and wall properties based on average values extracted from the scarce available literature. Although some of these assumptions may be acceptable in practice, no in-depth study has demonstrated their validity thus casting shadows on the accuracy of the current computational hemodynamics work. For this purpose a research consortium (**IRRAs** for **I**ndividual **R**isk **R**upture **As**sessment of Intracranial Aneurysm) was founded between 3 research Laboratories and 4 French neurosurgical centers (Montpellier, Lille, Nimes and Marseille) and involving corresponding departments of neuroradiology and anatomopathology. The first purpose of the **IRRAs** consortium is to build a database of aneurysmal biomechanical parameters. Such database will be instrumental in supporting new computational strategies to determine the risk of rupture in cerebral aneurysms based on patient-specific imaging data and domain-specific biomechanical knowledge.

The purpose of this study is to explore the biomechanical behavior characteristics of ruptured and unruptured aneurysms. Building such database is a mandatory to establish the idea that the rheology of the tissue correlates with the status of the aneurysm and that a biomechanical-based risk rupture factor can indeed be developed.

2. Materials and methods

2.1. Surgical technique and aneurysm selection

Eighteen patients treated for ruptured or unruptured aneurysms by surgical clipping were recruited by 4 French neurosurgical teams. The research study protocol was approved by the local ethical committee in each center. A consent form was signed by patients with normal neurological status, or by the relatives in all other cases. Following surgical clipping (Fig. 1) angio fluoroscopy imaging was performed by the neurosurgeon to control aneurysm sac exclusion. Once the distal aneurysm was confirmed to be safely excluded from the circulation, the neurosurgeons removed it in one piece. In this way, 18 intact aneurysms samples were then extracted from 17 patients.

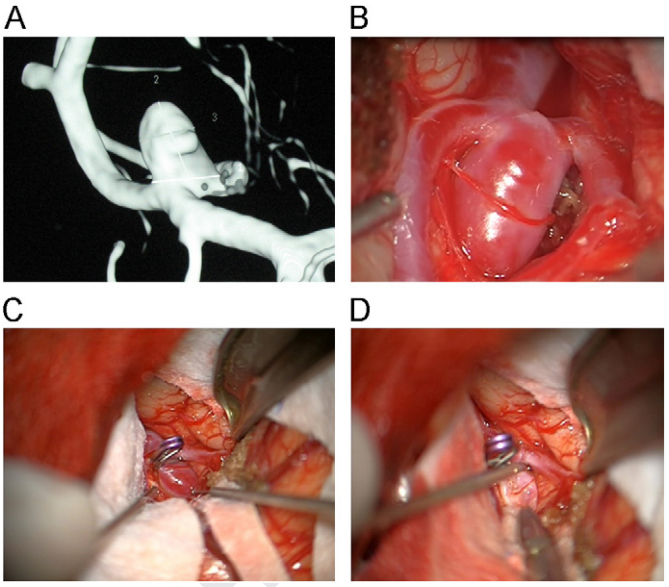

Fig. 1. (A) Three-dimensional rotational angiography imaging from Aneurysm #9. (B) Surgical view of this aneurysm in Middle Cerebral Artery location before clipping. (C) Aneurysm sac after surgical clipping. (D) Aneurysm resection.

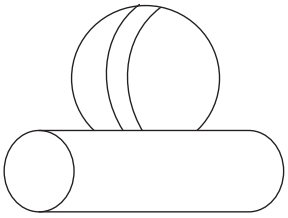

Fig. 2. Strips were cut out from the aneurysm sac following a meridional axis.

2.2. Clinical and radiological data

For each patient, clinical, and radiological information was collected concerning age, gender, aneurysm status (ruptured/unruptured), size (measured from the dome of the aneurysm and the neck represented by the communication of the aneurysm with the parent artery), the "dome to neck" ratio (aneurysm size/neck length), location on the Willis circle, morphological evaluation (classified "simple shaped" for regular unilobulated aneurysm and "complex shaped" for multilobulated and irregular aneurysm), as well as documented rupture risk factors; multiple aneurysms, previous ruptured aneurysm, positive family history of ruptured intracranial aneurysm, autosomal dominant polycystic kidney disease, hypertension, alcohol and tobacco. A possible mycotic intracranial aneurysm etiology was considered an exclusion criterion, as well as any previous history of endocarditis and inflammatory disease. All documented risk factors were then recorded in order to be related to the biomechanical behavior of each aneurysm.

2.3. Aneurysm sample conservation protocol

In order to conserve the mechanical properties of the aneurysm wall, a specific conservation protocol was applied in each center by means of a dedicated histopathological removal kit available in the neurosurgical operating room. The resected aneurysm was initially inserted in a tube containing a Ringer lactate, 10% DMSO solution. This first tube was then placed in a larger second one containing isopropanol. This combination of the two tubes was placed in a freezer (−80 °C). The sample was progressively frozen due to the surrounding isopropanol solution in order to maintain its biomechanical properties (Masson et al., 2009). Frozen samples were then stored in the anatomopathology department of the neurosurgical center, before mechanical testing was carried out.

Please cite this article as: Costalat, V., et al., Biomechanical wall properties of Human intracranial aneurysms resected following surgical clipping (IRRAs Project). Journal of Biomechanics (2011), doi:10.1016/j.jbiomech.2011.07.026

2.4. Biomechanical testing methodology

One hour before mechanical testing, aneurysms sample were thawed at ambient temperature. Under microscopy, the aneurysmal wall samples were dissected in a meridional manner in order to obtain a regular rectangular piece (Fig. 2). Only the meridional axis of the aneurysm was chosen in order to preserve maximum length of the aneurysmal tissue in the sample given the very small size of each specimen and the fragility of the tissue. The aneurysm strips were physically measured and then glued on each extremity to aluminum grips. Meanwhile, physiological isotonic liquid was warmed to 40 °C inside the traction test machine. A uniaxial stretch test was carried out on the sample within the warmed physiological liquid in order to simulate the in vivo conditions (Fig. 3A). This testing device was composed of a Texture Analyzer (TA-XT2, Stable Micro-systems, UK) with a 50 N load cell and an optical microscope (ZEISS) equipped with a digital video camera.

The uniaxial stretch test consisted of a sequence of 10% length displacement of the sample, in 5 repeated cycles (Fig. 3B), while registering the traction force applied. This 10% value was initially calculated by Karmonik et al. (2010) in an in-vivo wall motion MRI study of 7 aneurysms. In accordance to standard mechanical testing protocol for biological tissue, the specimens were first preconditioned (Holzapfel and Ogden, 2009) during the first four cycles. The extension rate was 0.01 mm/s and the tension load was recorded every 0.01 s. Velocity of the solicitations was small enough to not consider viscous phenomena. A baseline tension of 0 N was applied to the strip before starting each test, and two cameras were orthogonally placed and focused on the sample after a calibration test.

During the test, the two subset cameras were used to record the displacement of the sample. These images were subsequently used to determine the exact **dimensions** of the strips (resolution of 4μm/pixel). A Force/Displacement graph was obtained from each sample testing allowing tissue characterization.

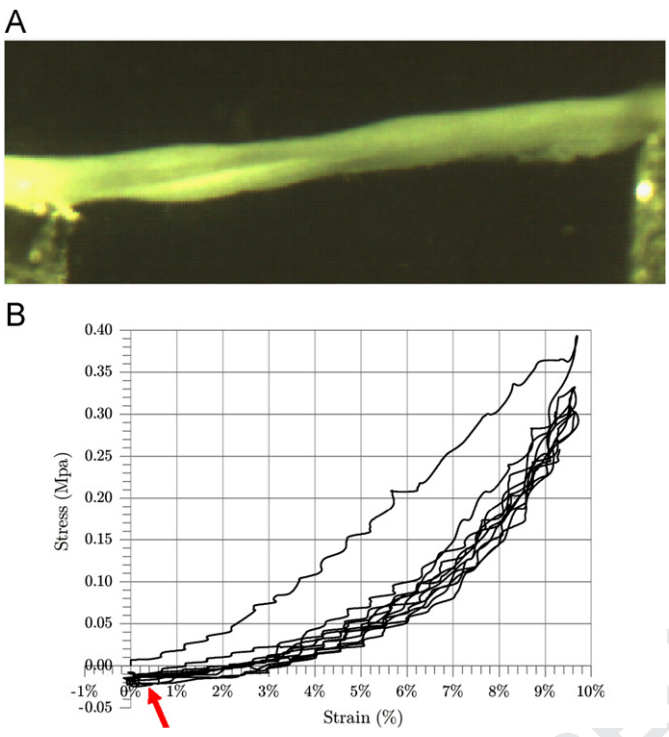

Fig. 3. Set-up and results from the uniaxial biomechanical testing. A. Side view of a wall strip from aneurysm n°4 during strain test, in a Ringer Lactacte solution at 40 °C. B. Strain/Stress graph. The hysteresis is observed between the first load (°) and the five cycles. A slight compression was observed during the rest phase due to micro structural changes of the sample during the first cycles leading to a permanent elongation. When coming back to initial size of the sample, a slight compression is then observed on the graph (arrow).

2.5. Post processing

Only the measurements from the last elongation cycle were used in order to obtain more realistic mechanical characterization of the data. Note however that except for the very first cycle, the force/displacement graph was roughly cycle independent (Fig. 3B). In order to tune the parameters of an equivalent hyper-elastic model, the force/displacement graph described above was converted in a strain/stress graph. For this calculation, the length, thickness and width of each strip were considered (Fig. 3B). A baseline for this aneurysmal **strip dimensions** were obtained at 0-Newton traction in the third cycle of each test. Using the assumption that the specimen was subjected to a uniform traction and presented a constant section during the test, the Cauchy stress was computed, and the engineering strain registered (Meyers et al., 2008; Oliver, 2006).

During the cycles some permanent deformation in the traction phase was observed causing slight compression of the sample in the rest phase. This is reflected by the negative values of the curve origin in Fig. 3b and is in accordance to the elasto-plastic behavior of the tissue. Since we consider an hyperelastic model to represent the tissue, the (moderate) plastic effects cannot be represented and only the positive part of the curve was used to identify material behavior.

Once the strain/stress graph was obtained, we proceed to a mathematical matching using a Sequential Least Squares Programming algorithm in order to determine the corresponding hyperelastic model and its coefficients. In our cases, the best match was obtained with a 3 parameters Mooney–Rivlin model (Mooney,

Table 1
Summary of clinical, anatomical and biomechanical data of the sixteen cases studied. (U=Unruptured, R=Ruptured, U-PRS=Unruptured with pre-rupture symptoms, MCA=Middle Cerebral Artery, PComA=Posterior Communicating Artery, ICA=Internal Carotid Artery).The tissue classification (Soft/Rigid/Intermediate) is done according to the graphs shown in Figs. 4 and 5.

Female Subgroup	Location	Cumulative documented risk factors	Aneurysm status	Thickness (μm)	Biomechanical properties	C_{10} (MR3) MPa	C_{01} (MR3) MPa	C_{11} (MR3) MPa	Statistical error
Aneurysm 3	MCA	0	**R**	420	Soft	0	0.0639	0.124	0.001
Aneurysm 4	ACA	2	**R**	300	Soft	0	0.0516	0.23	0.064
Aneurysm 16	ICA	1	**U-PRS**	380	Soft	0	0.04497	0.3077	0.00465
Aneurysm 6	PCA	5	**R**	450	Soft	0.02936	0	1.259	0.0355
Aneurysm 8	MCA	2	U	420	Intermediate	0.019057	0	2.196	0.0345
Aneurysm 11	MCA	5	U	390	Intermediate	0.0431	0	2.428	0.039
Aneurysm 10	ICA	5	U	310	Intermediate	0	0.0352	2.482	0.05
Aneurysm 15	PCA	1	U	680	Intermediate	0	0.06582	4.295	0.0433
Aneurysm 2	MCA	1	U	390	**Rigid**	0.376	0	**18.847**	0.033
Aneurysm 9	MCA	5	U	260	**Rigid**	0.2359	−0	**19.56**	0.049
Aneurysm 7	MCA	1	U	310	**Rigid**	0.7705	0	**32.149**	0.0067
Male subgroup	**Location**	**Cumulative documented risk factors**	**Aneurysm status**	**Thickness (μm)**	**Biomechanical properties**	**C_{10} (MR3) MPa**	**C_{01} (MR3) MPa**	**C_{11} (MR3) MPa**	**Stastistical error**
Aneurysm 5	ACA	1	**R**	330	Soft	0.1803	0	3.241	0.016
Aneurysm 13	ACA	1	**R**	290	Soft	0.9374	0	3.101	0.0267
Aneurysm 12	MCA	2	U	170	Intermediate	0.1951	0	14.987	0.0457
Aneurysm 14	MCA	1	U	200	Intermediate	0.1015	0	7.9232	0.04
Aneurysm 1	MCA	1	U	620	**Rigid**	0.2569	0	**12.265**	0.035

Please cite this article as: Costalat, V., et al., Biomechanical wall properties of Human intracranial aneurysms resected following surgical clipping (IRRAs Project). Journal of Biomechanics (2011), doi:10.1016/j.jbiomech.2011.07.026

1940; Rivlin, 1948). Let F be the measured load, S_0 the initial section and λ the elongation of the sample, the behavior law is given by the following equation:

$$\frac{F}{S_0} = 2(\lambda - \lambda^{-2})(C_{10} + C_{01}\lambda^{-1} + C_{11}(3\lambda^{-2} + 3\lambda - 3 - 3\lambda^{-1})) \quad (1)$$

where the material parameters are C_{10}, C_{01}, and C_{11}. The values of each of these coefficients for each aneurysm are gathered in Table 1 together with strip dimensions and relevant clinical factors.

2.6. Statistical analysis

The aneurysmal wall characteristics were presented using median and range for continuous variables and frequencies and proportions for categorical variables. Groups (defined by biomechanical status and material property) were compared using non-parametric Wilcoxon rank test for continuous variables and Fisher exact test for categorical ones. Statistical significance threshold was set at 5%. Statistical analyses were performed using SAS version 9.1 (SAS Institute, Cary, North Carolina).

3. Results

3.1. Population

Eleven unruptured and five ruptured aneurysms were included in the study. In one unruptured aneurysm case, pre-rupture symptoms with acute headache, and recent vision loss secondary to optic nerve compression was reported and highlighted in the Table 1. Mean age was 46.7 (min 32–max 64). Location was middle cerebral artery (MCA) in 9 cases (56.6%), anterior communicant artery (AComA) in 3 cases (18.7%), posterior communicant artery (PComA) in 2 cases (12.5%), and internal carotid artery (ICA) in 2 cases (6%). Aneurysm size is ranging from 4.2 to 13 mm.

3.2. Sample and mechanical testing

Out of the 18 aneurysms, 2 samples were not tested. In the first case, there were sample damages secondary to an error in the pretension setting of the hardware and in the second, sample loss in the operating room. Out of the 16 surgically clipped aneurysms that were subjected to mechanical uniaxial strain tests, 11 were from female and 5 from male patients (sex ratio = 0.45). Mean strip length was 4.8 mm (ranging from 1.3 to 8), with a mean thickness of 370 μm (ranging from 170 to 680 μm), and a mean section surface of 0.62 mm^2 (ranging from 0.29 to 1.6 mm^2).

Table 2
Comparison of clinical and biomechanical parameters between the three identified tissue subgroups in the overall population.

$n=16$	Aneurysmal wall biomechanical classification	n	Mean	p
Risk factors	Intermediate	6	2.6	0.456
	Soft	6	1.6	.
	Rigid	4	2	.
Wall thickness	Intermediate	6	360	0.994
	Soft	6	361	.
	Rigid	4	392	.
C_{10}	Intermediate	6	0.0598	0.057
	Soft	6	0.1911	.
	Rigid	4	0.3916	.
C_{01}	Intermediate	6	0.0168	0.792
	Soft	6	0.0267	.
	Rigid	4	0.0322	.
C_{11}	Intermediate	6	5.71	$<0.001^{**}$
	Soft	6	1.37	.
	Rigid	4	20.87	.

Q6

Table 3
Comparison of clinical data and biomechanical parameters between Ruptured and Unruptured aneurysms in the overall population (male and female).

	Status	n	Mean	p
Risk factors	**Ruptured**	6	1.66	0.366
	Unruptured	10	2.4	.
Wall thickness	**Ruptured**	6	0.36	0.918
	Unruptured	10	0.37	.
C_{10}	**Ruptured**	6	0.19	0.404
	Unruptured	10	0.19	.
C_{01}	**Ruptured**	6	0.026	0.757
	Unruptured	10	0.023	.
C_{11}	**Ruptured**	6	1.377	0.004^{***}
	Unruptured	10	11.78	

Table 4
Comparison of clinical data and biomechanical parameters between Ruptured and Unruptured aneurysms in the female group.

	Status	n	Mean	p
Risk factors	**Ruptured**	4	2	0.516
	Unruptured	7	2.85	.
Wall thickness	**Ruptured**	4	388	0.861
	Unruptured	7	392	.
C_{10}	**Ruptured**	4	0.00734	0.200
	Unruptured	7	0.20637	.
C_{01}	**Ruptured**	4	0.04012	0.279
	Unruptured	7	0.01443	.
C_{11}	**Ruptured**	4	0.48	0.001^{**}
	Unruptured	7	11.70	

The coefficient C_{10} value ranged from 0 to 0.9 Mpa with a mean value of 0.19 Mpa, C_{01} ranged from 0 to 0.13 Mpa with a mean value of 0.024, C_{11} ranged from 0.124 to 32 Mpa with a mean value of 7.87.

To facilitate analysis, aneurysms were classified according to their status Ruptured/Unruptured and their biomechanical behavior Rigid/Soft/Intermediate (see Tables 1 and 2).

Comparison of biomechanical parameters value among ruptured and unruptured aneurysms are summarized in Tables 3, 4, and 5.

4. Discussion

4.1. Results analysis

A recent case-control study (Low et al., 2011) on 4000 patients based on genetic variation suggests that the underlying mechanism for intracranial aneurysm pathogenesis may differ between male and female subjects, underlining the importance of a stratified analysis between genders. A significant difference in biomechanical parameters between ruptured and unruptured aneurysms was observed in our data within each gender group (Tables 3, 4, 5), therefore supporting the above statement.

Interestingly, the C_{11} coefficient, which represents the main curvature of each graph was the most representative parameter of this observed biomechanical difference (Table 3, $p<0.004$). The first two coefficients C_{01}, C_{10} presented a low value (near 0) and were not significantly different ($p=0.4$ and $p=0.7$) regarding aneurysmal status (ruptured/unruptured). All C_{11} values were

Please cite this article as: Costalat, V., et al., Biomechanical wall properties of Human intracranial aneurysms resected following surgical clipping (IRRAs Project). Journal of Biomechanics (2011), doi:10.1016/j.jbiomech.2011.07.026

observed below 1.2 MPa (mean 0.37 MPa) in ruptured or pre-ruptured female aneurysms, and below 3.2 MPa (mean 3.1 MPa) in male ruptured aneurysms.

In the female group, all the unruptured aneurysms presented a more rigid behavior than the ruptured or pre-ruptured aneurysms (C_{11}=0.48 vs. 11.7 MPa; $p<0.001$, Table 4). Between the unruptured aneurysms, we can distinguish two subgroups; the Unruptured/Rigid patients (#2-#7-#9) and the Unruptured/Intermediate patients (#8-#10-#11-#15). In this last subgroup representing an unruptured aneurysm with a softer aneurysmal wall, three out of four presented either documented major epidemiologic risk factors or a radiologically high risk shape (multilobulated). Only one aneurysm (#15) was simple shaped without further associated risk factors in this subgroup. One single patient (#16) presenting an unruptured aneurysm was classified as Soft with similar material properties with the Ruptured group. In this particular case, pre-rupture symptoms with major headache, and recent optic nerve compression were recorded few days before surgery and motivated urgent treatment. Therefore, in this case, the mechanical test findings of Soft may not be as paradoxical as thought of at the first glance.

Table 5
Comparison of clinical data and biomechanical parameters between Ruptured and Unruptured aneurysms in the male group.

	Status	n	Mean	p
Risk factors	**Ruptured**	2	1	0.495
	Unruptured	3	1.3	.
Wall thickness	**Ruptured**	2	309	0.638
	Unruptured	3	329	.
C_{10}	**Ruptured**	2	0.558	0.638
	Unruptured	3	0.160	.
C_{01}	**Ruptured**	2	−0.0001	0.638
	Unruptured	3	0.043	.
C_{11}	**Ruptured**	2	3.17	0.058
	Unruptured	3	11.95	.

In the male group, all the unruptured aneurysms tended have Rigid material than the ruptured ones (C_{11}=11.95 vs. 3.17 MPa; p=0.058, Table 5). Similarly to the female, unruptured aneurysms can be split in two subgroups, with 2 aneurysms classified Unruptured/Intermediate (Aneurysm #12 and #14), and one aneurysm classified Unruptured/Rigid. Among the Intermediate/Unruptured aneurysms one presented a major documented risk factor with multiple aneurysms, in accordance to a possible underlying connective tissue disease. Interestingly, in the male group, the ruptured aneurysms (Aneurysms #5 and #13) had a thicker wall compared to the Intermediate/Unruptured aneurysms, in contradiction to common conceptions, and in accordance to previous histoptahologic work (Crawford, 1959).

Rheological data relevant to aneurysmal tissue are very scarce in the literature. To the authors' knowledge, the only previous study is by Toth et al. (2007) who also gained insights about the tissue rheology from 1D traction testing. Unfortunately, no subgroup analysis among ruptured or unruptured status was performed by Toth et al. and the significant parameter C_{11} was not calculated. Still, the initial mean tangent modulus they obtained for their hyperelastic model can be compared to the $C_{01}+C_{10}$ parameter from the previous study. For the women group, this initial tangent modulus was evaluated from 2.79×10^{-2} to 22.4×10^{-2} Mpa vs. whereas it is in the range 1.905×10^{-2}–77.05×10^{-2} in our study. For the men group, this value was measured from 2×10^{-2} to 25.3×10^{-2} Mpa vs. from 10.15×10^{-2} to 93.74×10^{-2} in our study. From the results presented in this study, reproducible material characteristics were observed among the ruptured and pre-ruptured aneurysms with similar biomechanical behavior, suggesting a same vulnerable status of the aneurysmal wall in a rupture or pre-rupture status. These two behaviors were significantly different from the unruptured aneurysms, presenting a rigid tissue. At the same time, there was no statistical correlation observed between the thickness of the wall, the aneurysm size and the Ruptured/Unruptured aneurysms status. This observation supports the hypothesis that the aneurysm wall vulnerability is directly related to the tissue microstructure (Frosen et al., 2004), and not to a progressive wearing of the wall Figs. 4 and 5.

The evolution of aneurysmal biomechanical properties was modeled by Watton et al. (2009) who performed numerical

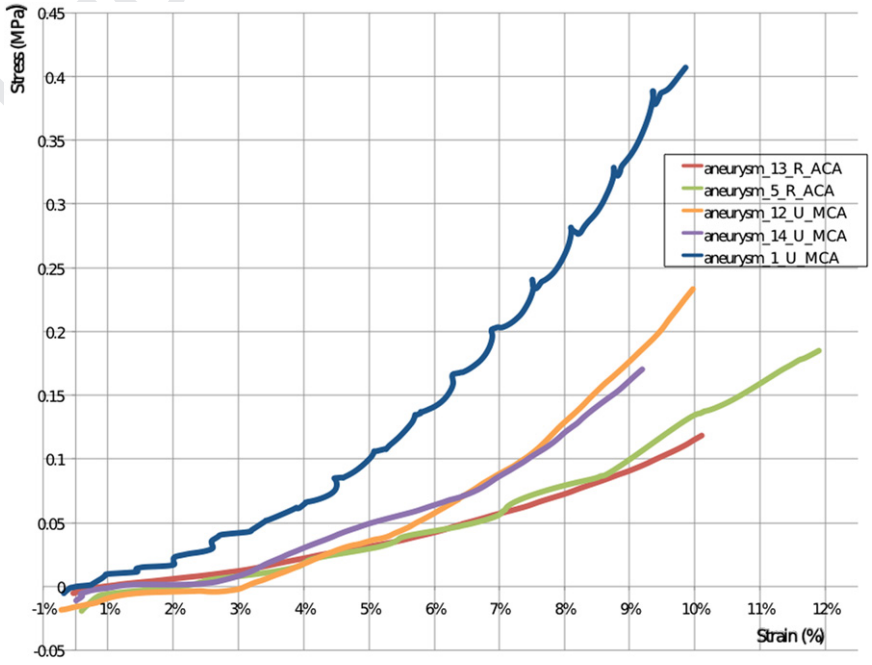

Fig. 4. Plots of the strain/stress relationships measured for men (R=ruptured, U=unruptured, ACA=Anterior Cerebral Artery, ACM=Middle Cerebral Artery).

Please cite this article as: Costalat, V., et al., Biomechanical wall properties of Human intracranial aneurysms resected following surgical clipping (IRRAs Project). Journal of Biomechanics (2011), doi:10.1016/j.jbiomech.2011.07.026

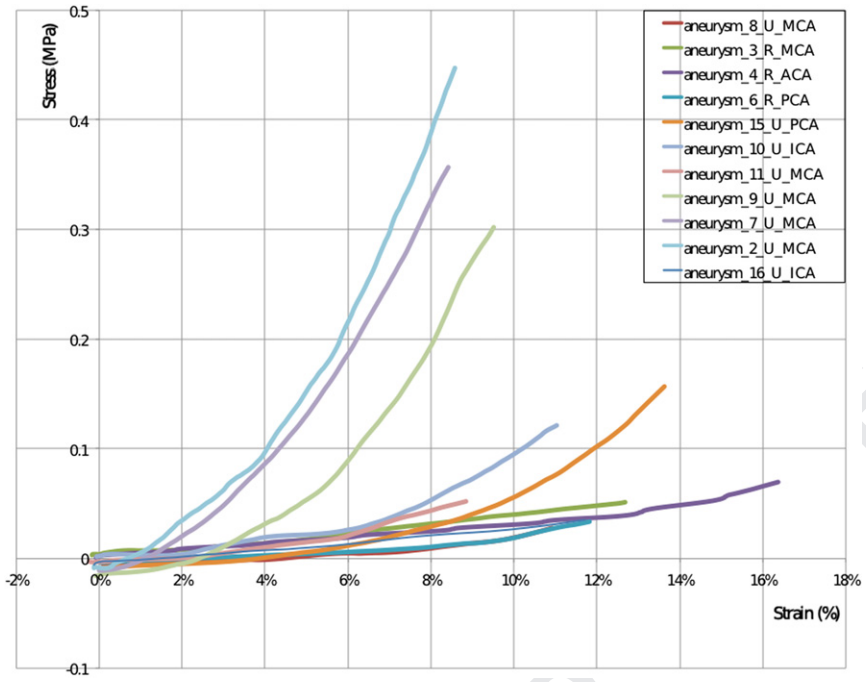

Fig. 5. Plots of the strain/stress relationships measured for women. (R=ruptured, U=unruptured, ACA=Anterior Cerebral Artery, ACM=Middle Cerebral Artery, ACI=Internal Carotid Artery, CPA= Cerebral Posterior Artery).

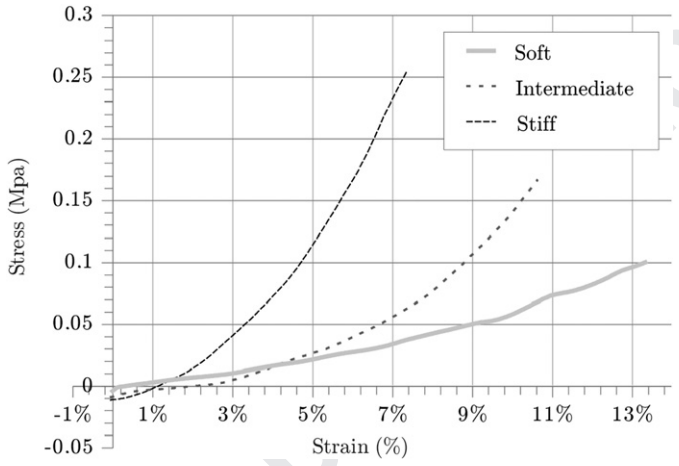

Fig.6. Mean strain/stress curves representing the biomechanical tissue classification.

simulations of aneurysmal initiation and growth and postulated a degradation model of the elastin layer. Furthermore, a previous histopathology study (Frosen et al., 2004) demonstrated that prior to rupture, the wall of cerebral aneurysm undergoes morphological changes associated with degeneration and repair.

The main contribution of our study has been to demonstrate a very significant biomechanical property difference between pre-rupture or rupture aneurysms with a soft tissue and unruptured aneurysm with a Rigid tissue (Fig. 6).

4.2. Limitation of the study

Because of the surgical resection necessary to obtain these samples, only aneurysms easily and safely accessible were selected, introducing a potential selection bias in this study. Hence, the MCA location was over-represented. There may be also a bias induced by the differences between cases with indication of surgical treatment compared to those indicated for interventional therapy. Nevertheless we observed aneurysm size ranging from 4.2 to 13 mm representing the majority of aneurysms treated to date. Within the statistical limitations of our sample, we could not observe any significant difference in mechanical properties of the aneurysmal wall according to the location. Interestingly, in the patient harboring two aneurysms (aneurysm #10 and #11) in different locations (ICA and MCA, respectively), we observed similar mechanical properties.

Uniaxial strain/stress testing is not representative of the anisotropic behavior of the aneurysm wall in vivo. Although, bi-axial testing was contemplated in this study, it is technically challenging to carry out. In our experiments the main limitation was the small size of the strips ranging from 1.2 to 8 mm. Work by Toth et al. (2007) also confirms that bi-axial testing does not generate reliable and reproducible results. MacDonald et al. (2000) investigated the molecular strength of the collagen fibers layers in 4 aneurysms. When comparing directional tissue strength, an anisotropy was demonstrated by a factor of 2. In our study, aneurysm samples were selected in a meridional direction in both groups demonstrating a difference between ruptured and unruptured aneurysm in this direction. A bi-axial testing of the sample would have been a response to this high level of anisotropy, but these tests were not possible in our experience due to the very small size of the aneurysms.

Furthermore, the probability of consistently and systematically slicing the aneurysm sample in the weakest direction in the ruptured aneurysms, and the strongest direction in unruptured aneurysms was unfeasible.

5. Conclusion

Gender stratification was necessary to interpret the biomechanical testing. Within each gender subgroup; ruptured aneurysms presented lower Rigidity than ruptured aneurysms, supporting the hypothesis that there is a change in the biomechanical properties of the aneurysm wall preceding rupture.

Please cite this article as: Costalat, V., et al., Biomechanical wall properties of Human intracranial aneurysms resected following surgical clipping (IRRAs Project). Journal of Biomechanics (2011), doi:10.1016/j.jbiomech.2011.07.026

Secondly, wall thickness was not correlated to ruptured/unruptured status. An Intermediate subgroup of unruptured aneurysms characterized by material properties corresponding to softer tissue was identified, and associated with multiple well documented risk factors of aneurysm rupture. Further studies about the biomechanical properties of cerebral aneurysms can help elucidating the biomechanical conditions preceding rupture. With the recent progress in in vivo aneurysm wall motion estimation (Karmonik et al., 2010; Zhang et al., 2009) it may be possible soon to estimate in vivo mechanical material properties of cerebral aneurysms (Balocco et al., 2010; Zhao et al., 2011). Such biomechanical parameters might be themselves good predictors of aneurysm rupture or might be integrated within a more comprehensive pipeline for image-based patient-specific simulations of fluid-wall structure interaction that renders a personalized estimate of the presence of vulnerable aneurysmal wall tissue and a potential increased rupture risk.

Conflict of interest statement

All authors do not have any financial and personal relationships with other people or organizations that could inappropriately influence this work.

Q2 Uncited references

Krings et al. (2009), Hayakawa et al. (2005), Ishida et al. (2005).

Acknowledgement

The authors would like to thank Philips™, Ansys™, for funding part of this research and providing free research software licenses. These sources of funding were not involved in the study design, in the collection, analysis and interpretation of data; in the writing of the manuscript; and in the decision to submit the manuscript for publication.

All authors have made substantial contributions to all of the following:

(1) the conception and design of the study; VC;DA;FJ;FN;MS
(2) acquisition of data; VC;MS; LT;NL;JPL;FS;HD;HB;PB;JPH;CAM; KK;AB
(3) analysis and interpretation of data; GM;VC;FJ;DA;MS
(4) drafting the article or revising it critically for important intellectual content; VC;MS;FJ;KL;DA;FN;LS;AFF

We certify that this manuscript has not been previously published, nor is being considered in whole or in part in any other primary scientific journal. All the authors are aware of and agree to the content of the manuscript. None of the authors have any conflict of interest to declare.

Q4 References

Anonymos, 1998. Unruptured intracranial aneurysms—isk of rupture and risks of surgical intervention. International study of unruptured intracranial aneurysms investigators. N. Engl. J. Med. 339, 1725–1733.

Asari, S., Ohmoto, T., 1993. Natural history and risk factors of unruptured cerebral aneurysms. Clin. Neurol. Neurosurg. 95, 205–214.

Alnaes, M.S., Isaksen, J., Mardal, K.A., Romner, B., Morgan, M.K., Ingebrigtsen, T., 2007. Computation of hemodynamics in the circle of willis. Stroke 38, 2500–2505.

Balocco, S., Camara, O., Vivas, E., Sola, T., Guimaraens, L., Gratama van Andel, H.A., Majoie, C.B., Pozo, J.M., Bijnens, B.H., Frangi, A.F., 2010N. Feasibility of estimating regional mechanical properties of cerebral aneurysms in vivo. Med. Phys. 37, 1689–1706.

Cebral, J.R., Castro, M.A., Appanaboyina, S., Putman, C.M., Millan, D., Frangi, A.F., 2005. Efficient pipeline for image-based patient-specific analysis of cerebral aneurysm hemodynamics: technique and sensitivity. IEEE Trans. Med. Imaging 24, 457–467.

Cebral, J.R., Mut, F., Weir, J., Putman, C., 2011. Quantitative characterization of the hemodynamic environment in ruptured and unruptured brain aneurysms. AJNR Am. J. Neuroradiol. 32, 145–151.

Cebral, J.R., Mut, F., Weir, J., Putman, C.M., 2011. Association of hemodynamic characteristics and cerebral aneurysm rupture. AJNR Am. J. Neuroradiol. 32, 264–270.

Crawford, T., 1959. Some observations on the pathogenesis and natural history of intracranial aneurysms. J. Neurol. Neurosurg. Psychiatry 22, 259–266.

Frosen, J., Piippo, A., Paetau, A., Kangasniemi, M., Niemela, M., Hernesniemi, J., Jaaskelainen, J., 2004. Remodeling of saccular cerebral artery aneurysm wall is associated with rupture: histological analysis of 24 unruptured and 42 ruptured cases. Stroke 35, 2287–2293.

Hoi, Y., Meng, H., Woodward, S.H., Bendok, B.R., Hanel, R.A., Guterman, L.R., Hopkins, L.N., 2004. Effects of arterial geometry on aneurysm growth: three-dimensional computational fluid dynamics study. J. Neurosurg. 101, 676–681.

Holzapfel, G.A., Ogden, R.W., 2009. Biomechanical Modelling at the Molecular, Cellular and Tissue Levels. CISM Courses and Lectures, 508. Springer, Wien, New York, pp. 259–343.

Hayakawa, M., Katada, K., Anno, H., Imizu, S., Hayashi, J., Irie, K., Negoro, M., Kato, Y., Kanno, T., Sano, H., 2005. Ct angiography with electrocardiographically gated reconstruction for visualizing pulsation of intracranial aneurysms: identification of aneurysmal protuberance presumably associated with wall thinning. AJNR Am. J. Neuroradiol. 26, 1366–1369.

Isaksen, J.G., Bazilevs, Y., Kvamsdal, T., Zhang, Y., Kaspersen, J.H., Waterloo, K, Romner, B, Ingebrigtsen, T., 2008. Determination of wall tension in cerebral artery aneurysms by numerical simulation. Stroke 39, 3172–3178.

Ishida, F., Ogawa, H., Simizu, T., Kojima, T., Taki, W., 2005. Visualizing the dynamics of cerebral aneurysms with four-dimensional computed tomographic angiography. Neurosurgery 57, 460–471 (discussion 460–471).

Kyriacou, S.K., Humphrey, J.D., 1996. Influence of size, shape and properties on the mechanics of axisymmetric saccular aneurysms. J. Biomech. 29, 1015–1022.

Karmonik, C., Diaz, O., Grossman, R., Klucznik, R., 2010. In-vivo quantification of wall motion in cerebral aneurysms from 2d cine phase contrast magnetic resonance images. Rofo 182, 140–150.

Krings, T., Willems, P., Barfett, J., Ellis, M., Hinojosa, N., Blobel, J., Geibprasert, S., 2009. Pulsatility of an intracavernous aneurysm demonstrated by dynamic 320-detector row cta at high temporal resolution. Cent. Eur. Neurosurg. 70, 214–218.

Low, S.K., Zembutsu, H., Takahashi, A., Kamatani, N., Cha, P.C., Hosono, N., Kubo, M., Matsuda, K., Nakamura, Y., 2011. Impact of limk1, mmp2 and tnf-alpha variations for intracranial aneurysm in Japanese population. J. Hum. Genet.

Masson, I., Fialaire-Legendre, A., Godin, C., Boutouyrie, P., Bierling, P., Zidi, M., 2009Progress. Mechanical properties of arteries cryopreserved at –80 degrees c and –150 degrees c. Med. Eng. Phys. 31, 825–832.

Meyers, Marc André, Chen, Po-Yu, Lin, Albert Yu-Min, Seki, Yasuaki, 2008. Biological materials: structure and mechanical properties, review article. Prog. Mater. Sci. 53, 1–206.

Mooney, M., 1940. A theory of large elastic deformation. J. Appl. Phys. 11, 582–592.

MacDonald, D.J., Finlay, H.M., Canham, P.B., 2000. Directional wall strength in saccular brain aneurysms from polarized light microscopy. Ann. Biomed. Eng. 28, 533–542.

Oliver, A., 2006. Shergold NAFaDR. The uniaxial stress versus strain response of pig skin and silicone rubber at low and high strain rates. Int. J. Impact Engi. 32, 1384–1402.

Radaelli, A.G., Augsburger, L., Cebral, J.R., Ohta, M., Rufenacht, D.A., Balossino, R., Benndorf, G., Hose, D.R., Marzo, A., Metcalfe, R., Mortier, P., Mut, F., Reymond, P., Socci, L., Verhegghe, B., Frangi, A.F., 2008. Reproducibility of haemodynamical simulations in a subject-specific stented aneurysm model–a report on the virtual intracranial stenting challenge 2007. J. Biomech. 41, 2069–2081.

Rivlin, R.S., 1948. Large elastic deformations of isotropic materials. I. Fundamental concepts. Philos. Trans. R. Soc. London A: Math. Phys. Sci. 240, 459–490.

Sluzewski, M., Bosch, J.A., van Rooij, W.J., Nijssen, P.C., Wijnalda, D., 2001. Rupture of intracranial aneurysms during treatment with guglielmi detachable coils: incidence, outcome, and risk factors. J. Neurosurg. 94, 238–240.

Scott, S., Ferguson, G.G., Roach, M.R., 1972. Comparison of the elastic properties of human intracranial arteries and aneurysms. Can. J. Physiol. Pharmacol. 50, 328–332.

Toth, B.K., Nasztanovics, F., Bojtar, I., 2007. Laboratory tests for strength paramaters of brain aneurysms. Acta Bioeng. Biomech. 9, 3–7.

Wardlaw, J.M., White, P.M., 2000. The detection and management of unruptured intracranial aneurysms. Brain 123 (2), 205–221.

Wiebers, D.O., Whisnant, J.P., Sundt Jr., T.M., O'Fallon, W.M., 1987. The significance of unruptured intracranial saccular aneurysms. J. Neurosurg. 66, 23–29.

Watton, P.N., Ventikos, Y., Holzapfel, G.A., 2009. Modelling the growth and stabilization of cerebral aneurysms. Math. Med. Biol. 26, 133–164.

Zhang, C., Villa-Uriol, M.C., De Craene, M., Pozo, J.M., Frangi, A.F., 2009. Morphodynamic analysis of cerebral aneurysm pulsation from time-resolved rotational angiography. IEEE Trans. Med. Imaging 28, 1105–1116.

Zhao, X., Raghavan, M.L., Lu, J., 2011. Identifying heterogeneous anisotropic properties in cerebral aneurysms: a pointwise approach. Biomech. Model. Mechanobiol. 10, 177–189.